# Conceptual Design of an Autonomous On-Orbit Refueling Spacecraft for Satellites in GEO

Aidan Kleinhenz, Nathan Belculfine, Camden Smith, Matthew Tannenbaum, Arin Magesh, Rishi Manoj

*H2Probe - University of Pittsburgh*



## Abstract

This paper presents the conceptual design of an autonomous spacecraft capable of performing in-orbit refueling and servicing of client satellites in geosynchronous orbit (GEO). The design addresses five major subsystem areas: a xenon propellant refueling system utilizing a bellow-driven accumulator for passive pressure-equilibrium transfer, a hexagonal docking mechanism with three spring-loaded capture claws, guidance navigation and control (GNC) for orbital rendezvous via Hohmann transfer, a regulated electrical power and dual-band communications architecture, and a hybrid-material chassis structure optimized for the GEO environment. Weighted trade studies were conducted for each subsystem to evaluate design alternatives against mission-driven criteria. The refueling system was validated through thermodynamic analysis using the Van der Waals equation of state and a MATLAB-based transfer simulation.

The resulting spacecraft concept demonstrates a feasible, modular, and maintainable platform for autonomous satellite servicing, advancing COSMIC's high-value mission objectives for in-space servicing, assembly, and manufacturing.

## Nomenclature

### Propellant & Thermodynamics

P — Pressure (MPa)

T — Temperature (K)

V□ — Molar volume

a, b — Van der Waals constants

R — Universal gas constant

$T_c$ — Critical temperature

$P_c$ — Critical pressure

$P_{pre}$ — Bellows pre-charge pressure

$P_{min}$ / $P_{max}$ — Minimum/maximum xenon pressures across GEO temperature range

$P_f$ — Final equilibrium pressure

$P_b$ — Bellows pressure

$P_C$ — Client tank nominal pressure (pre-transfer)

$V_{acc}$ — Accumulator volume

$V_x$ — Propellant (xenon) volume

$V_b$ — Bellows volume

$V_C$ — Client tank volume

k — Nitrogen gas isentropic exponent

### Structures & Materials

$r_o$ — Outer radius (m)

$r_i$ — Inner radius (m)

$\rho_{CFRP}$ — Density of Carbon Fiber Reinforced Polymer (kg/m³)

$\rho_{Ti}$ — Density of Ti-6Al-4V

V — Volume of hollow cylinder (m³)

$m_{spine}$ — Mass of central spine (kg)

$m_{bulk}$ — Mass of forward docking bulkhead (kg)

A — Bulkhead area

t — Bulkhead thickness

α — Coefficient of thermal expansion (CTE)

ΔT — Change in temperature

k — Thermal conductivity

q — Heat flux

∇T — Temperature gradient

**Acronyms**

GEO — Geosynchronous Orbit

MEO — Medium Earth Orbit

LEO — Low Earth Orbit

GNC — Guidance, Navigation, and Control

ISAM — In-Space Servicing, Assembly, and Manufacturing

CONOPS — Concept of Operations

PMAD — Power Management and Distribution

PCU — Power Conditioning Unit

HGA — High Gain Antenna

LGA — Low Gain Antenna

CFRP — Carbon Fiber Reinforced Polymer

MLI — Multi-Layer Insulation

P&ID — Piping and Instrumentation Diagram

PDR — Preliminary Design Review

NDS — NASA Docking System

CTE — Coefficient of Thermal Expansion

TT&C — Telemetry, Tracking, and Commanding

## Introduction

Satellites in geosynchronous orbit represent investments often exceeding $500 million, yet most become inoperable due to propellant depletion or component degradation rather than catastrophic failure. The typical GEO satellite has a design life of 10–15 years, but residual capability often remains after its primary mission ends. On-orbit servicing offers a cost-effective alternative to full satellite replacement by extending mission lifetimes through refueling, inspection, and component augmentation at a fraction of the cost and time required to design, build, and launch a replacement.

This paper responds to the COSMIC Capstone Challenge Track 3 prompt: to design a modular and maintainable spacecraft capable of autonomously servicing multiple client satellites to provide critical servicing functions. The spacecraft is designed to autonomously rendezvous with, dock to, and refuel client satellites in GEO using xenon propellant. The design emphasizes modularity, maintainability, and compatibility with existing and future satellite architectures.

Key subsystems include a bellows-driven refueling system, a three-claw hexagonal docking mechanism, dual-band S/X-band communications, triple-junction GaAs solar arrays with a regulated power bus, and a hybrid CFRP/aluminum/titanium central-spine chassis. Each subsystem was developed through weighted trade studies comparing multiple design alternatives, and key systems were validated with analytical models in Excel and MATLAB.

The following sections detail the design methodology, trade study results, and analysis for each subsystem, followed by a concept of operations overview, risk assessment, data handling architecture, lessons learned, and a recommended path to Preliminary Design Review (PDR).

## 1. Refueling System

The lifespan of satellites and spacecraft in geosynchronous orbit (GEO) rely heavily upon electric propulsion, specifically hall-effect thrusters and gridded-ion thrusters. These propulsion systems are most commonly fueled by noble gases such as xenon and krypton, stored in a supercritical state to avoid active cooling and cryogenic conditions. For a refuelling operation to be successful, it is crucial that the propellant is kept in a supercritical state by staying above its critical pressure and temperature during storage up until its transfer into the client's fuel tank. To achieve this, an accumulator consisting of a gas pre-charged bellows was identified to be capable of storing the propellant with a driving pressure to efficiently transfer the propellant once our spacecraft is interfaced with the client's tank [1]. This transfer can occur through the expansion of pre-charged bellows, caused by the difference in pressure to the client's tank, with propellant as the median. For this to be successful, the client's tank pressure must be monitored and pressurized or vented to a nominal pressure before releasing our valves to allow the equilibrium pressure between the two systems to be reached, while maximizing the mass of propellant transferred. To operate this system, the main subsystems consist of an accumulator pre-charged with a bellows and propellant, a high-pressure helium gas cylinder, and propellant and gas feed lines routed through an interface with dedicated gas and propellant feed ports. This interface will be integrated onto the client spacecraft/satellite prior to launch, enabling on-orbit refueling upon rendezvous.

### 1.1 Trade Study of Alternative Propellants

Determining the most suitable propellant for on-orbit refueling missions in GEO requires a structured trade study that evaluates candidate propellants across servicing-driven criteria—including technological maturity and compatibility, cost and availability, storage and transfer capability, and propellant density.

Technological maturity and compatibility was the first criterion identified, knowing that our refueling services would be opportunistic and limited to client systems that utilize the selected propellant type, and was weighted at 0.30. Storability and transferability was weighted at 0.30 as well, due to the main operation of our service depending on these characteristics. Cost and availability was selected as the third criterion, weighted at 0.25. Finally, density was identified as a criterion to evaluate the mass of propellant able to be transferred to systems subject to small fuel tanks, and was assigned a weight of 0.15.

Each propellant alternative was evaluated using a normalized scaling approach, where the score was calculated as ten times the ratio of the candidate propellant's characteristic value to the maximum desired value observed among all alternatives for that criterion. For maturity and compatibility, NASA's State-of-the-Art report on in-space electric propulsion was referenced [2], with xenon being the most common and krypton scoring competitively. For storability and transferability, xenon was recognized as the most exhibited and successfully stored propellant in GEO missions, while iodine's solid storage and heated feed requirements present greater complications for refueling operations. For cost and availability, iodine was the least expensive, followed by krypton, and xenon being the costliest [3, 4]. Density was evaluated at equivalent storage conditions, with iodine ranking highest and krypton lowest [5].

As a result, xenon scored the highest out of the evaluated propellant alternatives, driven by its maturity and compatibility in current GEO missions. While krypton and iodine offer advantages in cost, availability, and density, their low flight heritage and refueling complications led to lower overall scores.

**Table 1. Weighted Propellant Trade Study for On-Orbit Refueling in GEO**

| | Maturity & Compatibility (0.30) | Storability & Transferability (0.30) | Cost & Availability (0.25) | Density (0.15) | Score: |
|---|---|---|---|---|---|
| **Xenon** | 10 | 9 | 1 | 3 | 6.40 |
| **Krypton** | 4 | 7 | 9 | 1 | 5.70 |
| **Iodine** | 1 | 2 | 10 | 10 | 4.90 |

## 1.2 Propellant Storage and Transfer Analysis and Methodology

To determine the exact properties of xenon's state throughout this operation, Excel was used to organize the data and dependent cells with necessary equations and reliance on specific properties. Throughout the analysis, the Van der Waals Equation of State (EOS) was used as a function, dependent on temperature, to determine the pressure of xenon at various periods of the operation.

$$P = \frac{RT}{V_m - b} - \frac{a}{V_m^2} \qquad (1)$$

$$a = \frac{27R^2T_c^2}{64P_c}$$

$$b = \frac{RT_c}{8P_c}$$

Specifically, the main periods of pressure computation occur at the immediate temperature upon the transfer operation, as well as the highest and lowest expected temperatures to be reached throughout the entirety of the operation. To properly size the accumulator and achieve our bellows' gas pre-charge pressure, a common sizing equation was used that utilizes the minimum and maximum pressures that are expected from the extreme range of temperatures our spacecraft may experience [6]. Furthermore, the equation inputs the nitrogen gas isentropic exponent as well as our propellant volume and accumulator volume. Following a common ratio of 2:1 for accumulator (total volume, fluid + bellows) to fluid/propellant volume and the initialized volume and density of our propellant for our desired mass transfer of 210 kg, the accumulator volume was yielded as a volume of 0.3 $m^3$ with its volume split (0.15 $m^3$ each) to the bellows and propellant volume. To ensure the accumulator sizing equation is valid across all possible refueling missions, the maximum and minimum xenon pressures are evaluated using Eq. (1) at the extreme temperatures characteristic of GEO [7]. Rearranging the equation, the pre-charge pressure of nitrogen gas within the bellows was determined to be 6.84 MPa.

$$P_{pre} = P_{min} / [\frac{V_{acc}}{V_x}(1 - (\frac{P_{min}}{P_{max}})^{1/k})]^k \qquad (2)$$

Once our spacecraft is docked with the client's tank via interface connection, the client tank pressure must be brought up to a nominal pressure that allows the transfer of the propellant to be completed with a final equilibrium pressure between the bellows and the client tank above the critical pressure of xenon. To find this nominal pressure, the bellows and client tank are conceptualized as a connected two-volume system with differing respective initial pressures, which allows the use of an ideal gas equilibrium pressure equation. The final equilibrium pressure of 7.11 MPa was equated using the ideal gas law equation of the nitrogen pre-charged bellows with a volume of the full expansion size, as the total accumulator size, to maximize the amount of propellant transferred. Then, the nominal pressure of the client tank ($P_C$), before the transfer occurs, is calculated. This equation is dependent on the size of our client's tank, so the input volume ($V_C$) can be changed for a given refueling mission.

$$P_C = \frac{P_f(V_b + V_C)}{V_C} - \frac{P_b V_b}{V_C} \qquad (3)$$

This nominal pressure or pre-pressurization can be reached through methods of venting if the pressure is too high, or supplying pressure from a high-pressure helium gas cylinder within our spacecraft. With the final volume of the bellows, the final volume and mass of the xenon within our accumulator can be yielded. Subtracting from the total mass of xenon originally in the accumulator, the amount transferred into the client tank is equated.

## 1.2.1 Matlab Model of Simulated Scenario

To visualize the transfer process, a model was created using MATLAB with realistic conditions for a simulated scenario of this operation. Specifically, the ambient conditions' effects on our spacecraft and internal xenon can be exemplified as a temperature of 310 K, causing a pressure of 13.4 MPa using Eq. (1). Additionally, the client tank volume will be known, which is 0.2 m³ in this example, resulting in a nominal client pressure of 2.4 MPa. The pressure equalization between the accumulator and client tank was modeled using a first-order exponential decay response, where the resulting bellows expansion drives the mass transfer of xenon into the client tank over the duration of the operation.

**Figure 1. Xenon Transfer Pressure vs Time**

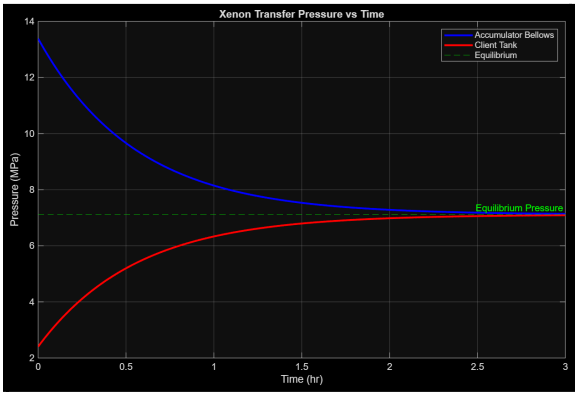


**Figure 2. Xenon Mass Transfer vs Time**

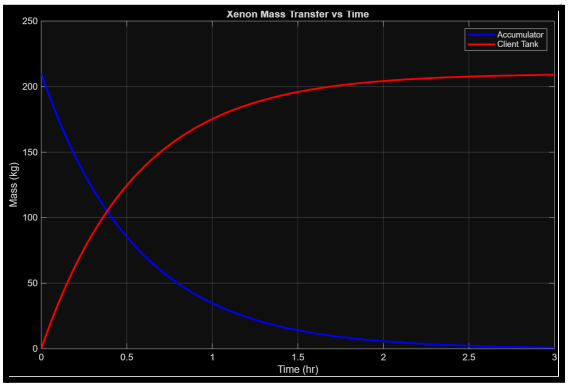


## 1.3 System Layout and Architecture

The P&ID of the proposed refueling system, docked with the client tank, is shown in Fig. 3, detailing the arrangement of gas and propellant feed lines and the necessary instrumentation to operate the refueling procedure. The operational sequence of the refueling system once our spacecraft is docked with the client is illustrated in Fig. 4, outlining the process of monitoring the client tank, inducing it to nominal pressure, and valve control to allow the transfer to occur.

**Figure 3. P&ID - Refueling System**

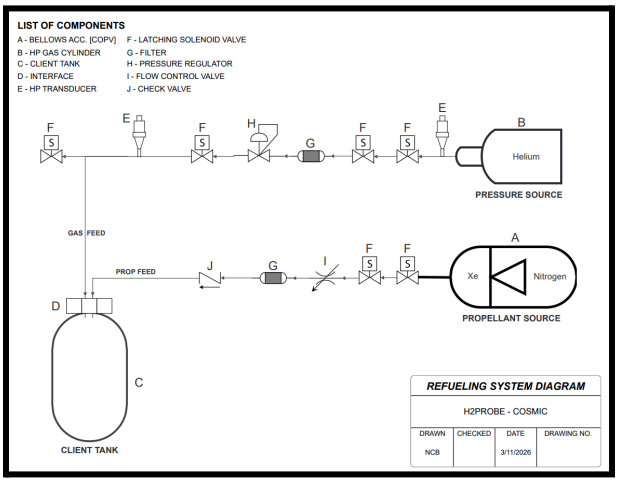

**Figure 4. Refueling Operations Flow Diagram**

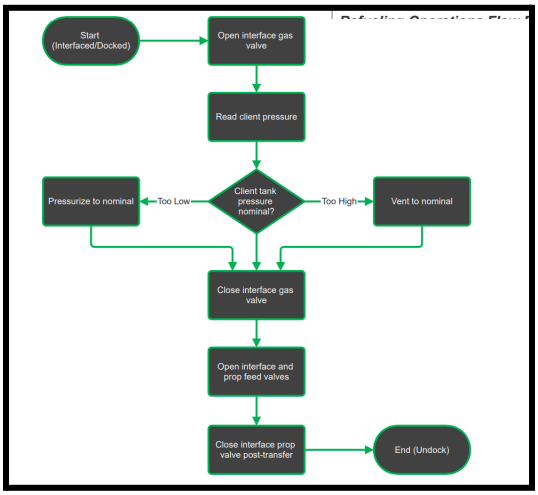


## 2. Docking System

On-orbit autonomous refueling missions rely on the ability of two spacecraft to form a controlled and reliable connection in space. This fact makes the docking procedure one of the most critical subsystems in any satellite servicing mission. The docking procedure consists of the servicing satellite to approach the client satellite at extremely low velocity (~5 cm/s), initial capture of the client, alignment correction, and finally hard capture connection. Unlike terrestrial docking, Geosynchronous orbit (GEO) rendezvous requires low impact energy and near-perfect alignment. To address these challenges, modifications were made in previous missions to confirm a successful transfer of fuel. A trade study was conducted to compare potential designs, with a CAD model presenting the final design.

### 2.1 Trade Study of Capture Phases

The ability to dock a refueling satellite with a client satellite is a fundamental mechanism that enables a successful mission when performed correctly. Candidates in this study must meet the basic requirements of including both soft-capture and hard-capture functionality, operating in geosynchronous orbit, and being cost effective. Based on these requirements, three candidates were selected for evaluation using a weighted criteria set. The following criteria were scored on a numerical scale and multiplied by their assigned weights to determine an overall ranking.

The first criterion used to test each system was configuration displacement tolerance, weighted at 10%. This criterion was weighted lowest because if the Guidance, Navigation, and Control (GNC) system performs as intended, then large interface offsets should be uncommon. The NASA Docking System (NDS) uses a soft capture phase to “catch and lunge” toward the client satellite, using electromechanical actuators to align the docking interfaces before retracting the actuators to complete the capture sequence [8]. Orbit Fab’s RAFTI+GRIP design recorded a similar placement to the SM design due to their similarity in capture mechanisms. Both systems rely on a claw-style mechanism that attaches to the client interface and draws the satellites together, providing less misalignment tolerance than NDS [9]. However, the modeled SM system includes an added mechanism that extends the claw arms outward, increasing the effective grapple radius.

The second criterion chosen to compare designs was compatibility, weighted at 35%, making it the second most important factor in the selection process. The ability for the servicing satellite to dock with a variety of client satellites and interface types is an essential driver for mission feasibility. The NDS is a standardized docking system designed primarily for spacecraft docking and crewed operations. However, it is not typically implemented for autonomous refueling applications, which reduces its applicability to this mission [8]. Due to this factor, the NDS scores a 2 for compatibility. Orbit Fab’s system, in contrast, is designed specifically for autonomous in-space refueling. Thus, the system was given an 8 due to its relevance to autonomous servicing and its ability to support refueling operations across multiple clients. The SM model scored a 10 on compatibility due to its similarity to Orbit Fab’s GRIP mechanism, while also incorporating an extended grapple radius that may increase compatibility with interfaces beyond

its manufactured counterpart. The SM model could potentially dock with RAFTI-like targets and other similar refueling ports.

The third criterion used to test designs was energy absorption capability, weighted at 20%. This weight was selected because docking and refueling operations are expected to occur at low contact velocities (on the order of mm/s to cm/s), reducing the total kinetic energy involved at contact. The NDS demonstrated the highest energy absorption capability due to its soft capture ring and electromechanical actuation system, initially capturing clients and absorbing remaining kinetic energy [8]. Because of this capability, the NDS was given an 8 for energy absorption. Orbit Fab's RAFTI+GRIP system is designed for slower, more precise rendezvous and capture operations, placing less emphasis on large-stroke energy attenuation and receiving a score of 7 [9]. The SM model is expected to operate under similarly low-velocity capture conditions, leading to the same overall conclusion regarding kinetic energy. Due to its similarity to the RAFTI+GRIP approach, the SM model also scored a 7 for this criterion.

The fourth and final criterion was cost, weighted at 35% due to its high impact on mission feasibility. Cost can be the difference between a project moving forward or failing to progress beyond early development. However, lowest cost does not necessarily indicate the best overall solution, which is why the criteria were weighted to account for performance trade-offs. The NDS scored the lowest overall cost score, receiving a score of 5, since the estimated system cost is approximately $14–$18 million USD [8]. For the purposes of this mission, the NDS is not cost effective. The RAFTI+GRIP system scored similarly to the SM model. The RAFTI interface is publicly listed at $30,000, while the cost of GRIP is not publicly listed. Based on internal estimates, the combined system cost is assumed to fall between $10–$12 million USD [9]. The SM system is estimated to reduce the interface cost by approximately half of the RAFTI listed value while maintaining similar operational capability. Because the SM claw mechanism is similar in function to GRIP, its cost is assumed to remain comparable, making the SM system slightly more cost effective overall.

As a result of this Trade Study, the clear winner was the SM model. The NDS model placed last due to their system being crew-member based and our needs being autonomous refueling. Orbitfab's RAFTI+GRIP was second with a great autonomous refueling design that could only be slightly improved. Taking all considerations into account, it makes sense to go forward with the SM model.

**Table 2. Weighted Autonomous Refueling Docking System Trade Study**

| Trade study | Displacement Tolerance (.10) | Compatibility (.35) | Energy Absorption (.20) | Cost (.35) | Results |
|---|---|---|---|---|---|
| NASA (NDS) | 10.0 | 2.00 | 8.00 | 5.00 | 5.05 |
| Our Design | 7.50 | 10.0 | 7.00 | 10.0 | 9.15 |
| Orbitfab's RAFTI | 7.00 | 8.00 | 7.00 | 9.50 | 8.30 |

## 2.2 Docking Methodology

The docking procedure must be explained, in hopes of providing some context for certain design decisions. The SM design seeks to act as a servicing satellite, approaching and latching onto the client satellite. As a result, all design decisions account for the active nature of the SM system.

In order to determine the best design style possible, shapes needed to factor in low material usage and costs, while also having a robust and flexible design. In searching for a shape, a square was initially considered, but the surface area and rigid nature of the shape made it hard to justify its applicability across varying degrees of client interfaces. Instead, after multiple iterations, a hexagonal structure was chosen to serve as the base of the servicing interface. The hexagonal structure saves on some costs that would have been present with a square design, while providing the robust

compatibility with a number of different client satellites that a circle also had.

Inspired by the structure of traditional three-pronged grasping mechanisms, the decision to utilize three claws as opposed to two or four comes down to the balance between maintaining low material usage and costs, while providing a great enough surface area when latching onto the client satellite. The face of the hexagon is faceted with three claws, 60 degrees apart from each other. Traditional capture phases use rectangular latches to lock the client and the servicer to each other, discouraging adjustment or movement after successful rendezvous connection, meaning that small misalignments can have devastating effects on the docking process. Therefore, as a means of addressing and seeking to correct this issue, a claw system was chosen to replace the traditional latches. The three claws each are capable of extending, giving the servicing satellite room to make micro adjustments depending on the position of the client satellite. This change is not meant to eliminate the precise maneuvering of the autonomous system, but rather, provides a buffer so that should the system fail or have trouble aligning, the claws can act as an extra layer of security.

As the servicing satellite approaches the client satellite, each arm extends outwards at approximately 25 mm, with a maximum radius of 97.7 mm achieved at full extension. The claws are dispersed as the client is initially captured. Again, the dispersion of these claws do not necessarily always need to be fully extended, but the range provides a greater degree of flexibility.

Before hard capture can begin, correct alignments must be assessed and corrected. The claws are a little bit larger than the client, ensuring that there is enough room for tweaking alignment prior to initiating hard capture. In order to account for this extra space, each claw is also outfitted with a square groove within its inner face. These grooves make sure that despite any alignment changes, the claws will be firmly locked into place on the client satellite. The decision to include these groovers were not included in the initial design and ideation process, but came about as a way of further securing the two satellites to each other. Modeled after the NDS fine alignment pins, these grooves are small indentations.

Finally, when hard capture connection is confirmed, the spring-loaded locking mechanisms on each claw fall into place. The hallmark of the SM design, the spring-loaded locking mechanisms are blocks that remain in a neutral state prior to the latching of servicing and client, similar to and modeled after the click of a ballpoint pen. Once successful rendezvous connection has been reached, each springloaded block will engage with its corresponding interface and signal the complete connection between servicer and client. The spring-loaded locking mechanisms are an answer to the traditional docking and undocking springs present on most docking systems. They are meant to serve as a final point of contact for the docking system, for both docking and potential release from the client. Therefore, the decision to include them was spurred by a need to be able to latch as well as release the servicing satellite from the client when needed. Traditional springs offer a similar functionality, but fall short in low material fatigue, due to the added stresses placed on them over time. In comparison, the spring-loaded locking mechanism locks in and out depending on whether or not it is engaged. This greatly reduces overall force applied to the spring, as force is only applied when needed.

**Figure 5. Docking Mechanism System Layout**

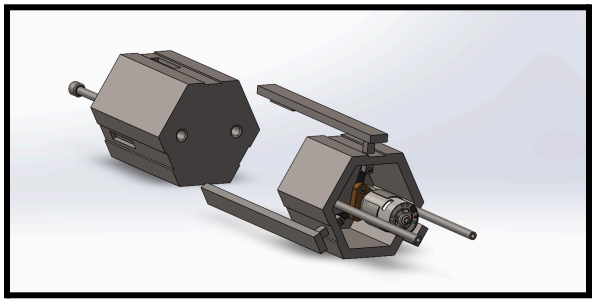

## 3. Overview of the Chassis Structure

The chassis structure of the small satellite serves as the interface for all ISAM operations, the structure that holds all the satellite subsystems together, and the support structure during launch and docking.

For a spacecraft operating in the geosynchronous orbit (GEO), the structure must be durable and maintain structural alignment throughout the launch, docking, and its journey through space in between. It must also withstand extreme environmental conditions, one being large thermal swings. Through its traversal to the GEO, the spacecraft may experience external temperatures ranging from approximately −150°C to +150°C [10]. Another condition to consider is radiation exposure; on its trip to GEO, the spacecraft would have to pass through both the Van Allen radiation belts, which extend from roughly 1,000 km to 60,000 km in altitude and contain trapped, high-energy charged particles. Within these regions, proton fluxes can reach on the order of $10^8$ protons/cm²·s, making radiation mitigation a necessary condition to satisfy during structural design [11].

The chassis needs to support the satellite, align for docking, manage temperature changes, insulate against extreme heat and cold, and shield from radiation.

### 3.1 Trade Study of Structures

For the structures trade study, three commonly used structural configurations in small satellites were considered: a central load-bearing spine, a monocoque shell, and a truss structure. A central load-bearing spine consists of a thick-walled tube or rectangular prism, with launch loads going straight through it, and the docking ring bolting to the end. A monocoque shell is a structure in which the spacecraft's outer skin serves as the primary structure, while also supporting ring frames within. The docking ring would likely be in the forward end bulkhead of the satellite. A truss structure consists of a group of trusses joining to form the structure of the spacecraft.

Three real-life satellites that fall into the categories, to provide a basis for comparison: Northrop Grumman MEV for the spine, ESA ATV pressurized module for the shell, and the NASA Hubble Space Telescope [12][13][14][15]. These three structures were evaluated using six metrics. First, structural efficiency, which is how much load the structure can hold for a given mass. Second, stiffness, which measures how well the structure can resist bending and twisting from forces experienced in docking a satellite. Third, docking path clarity; basically, how easy is it to predict the direction and magnitude of the forces exerted on the chassis when it does? This allows us to strengthen and reinforce the parts of the satellite under the most pressure. Fourth, replaceability: how easy is it to modify the spacecraft during the testing phases without redesigning the entire structure? Fifth, manufacturability, which is how easy it is to build the satellite. Finally, reliability: how proven is the architecture in docking and GEO missions? Categories were weighted 25, 25, 20, 15, 10, and 5, respectively. This criterion was determined by the mission's requirements: to create a rigid smallsat capable of traversing to the GEO and withstanding the forces associated with the docking process. Structural efficiency and stiffness were weighted most heavily due to the importance of durability, whilst also minimizing costs and drag by maintaining a smallsat with minimal mass. Another important factor would be docking path load clarity at 20%, since a clear load path facilitates easier stress analysis and reduces the risk of misalignment. Ease of making iterations to the spacecraft, while important, isn’t as pressing as the spacecraft's durability, and thus was assigned 15%. Manufacturability and reliability were weighted the least because, while important, each of the analyzed spacecraft has some level of heritage, thus serving as a secondary discriminator rather than a primary metric.

For the results, the results were linearly scaled by taking 10 and multiplying it by the quotient of that spacecraft’s results divided by the maximum results overall. The metrics used to evaluate these criteria are as follows: Normalized

structural mass factor (for this one, the lower the better, so the scaling used was the minimum results overall divided by the spacecraft's results), normalized bending stiffness, % of docking load entering a single primary structure, number of predefined load-rated beams, normalized complexity index and % heritage in similar mission class. Results were then multiplied by each category's weight and summed across all categories for the spacecraft to obtain an objective score for the best chassis structure for the mission. After calculations were completed, the results were as follows: Spine - 8.96/10, Shell - 7.08/10, Truss - 8.74/10. Thus, a central load-bearing spine, with a ring attached to the posterior of the structure, would be most effective for this mission.

**Table 3. Chassis Structure Trade Study for On-Orbit ISAM missions in GEO**

| Criterion | Wt | A1 Spine | A2 Shell | A3 Truss |
|---|---|---|---|---|
| **Structural Efficiency** | 25% | 8.33 | 7.41 | 10.00 |
| **Stiffness / Alignment** | 25% | 9.00 | 7.50 | 10.00 |
| **Docking Load Path Clarity** | 20% | 10.00 | 6.67 | 6.11 |
| **Replaceability** | 15% | 7.50 | 5.00 | 10.00 |
| **Manufacturability** | 10% | 10.00 | 8.80 | 6.88 |
| **Reliability** | 5% | 10.00 | 7.78 | 6.67 |

Totals: A1 - 8.96/10, A2 - 7.08/10, A3 - 8.74/10

## 3.2 Trade Study of Structural Materials

Following the selection of the structural architecture, a second trade study evaluated candidate materials for the spacecraft structure. Four commonly used materials for aerospace structures were considered: Aluminum 6061-T6 – A high strength aluminum containing magnesium and silicon that's heat treated, Aluminum 7075-T6 – A High strength aluminum alloy, mainly alloyed with zinc that's heat treated, Ti-6Al-4V – A Titanium alloy, alloyed with 6% aluminum and 4% vanadium, and Carbon Fiber Reinforced Polymer (CFRP) – Layers of carbon fiber fabric embedded in epoxy. These four structures were evaluated using 4 metrics. First, the strength-to-weight ratio is weighted at 31.25%, which measures how efficiently a material can support a load relative to its mass. The second, dimensional stability, also weighted at 31.25%, determines the material's resistance to thermal deformation. Next is thermal spreading, weighted at 18.75%, which measures the material's ability to conduct and distribute heat across the small satellite. Finally, radiation shielding efficiency, weighted at 18.75%, which evaluates the material's ability to attenuate radiation per unit thickness.

### 3.2.1 Determining Strength-to-Weight Ratio

The strength to weight ratio was measured by taking the yield strength of the material and dividing it by material density.

It can be modeled through the equation:

$$R = \frac{\sigma_y}{\rho}$$

**Table 4. Yield Strength and Density of Materials [16][17][18]**

| Material | Yield Strength (MPa) | Density (g/cm^3) | Ratio |
|---|---|---|---|
| Al-6061-T6 | 276 | 2.70 | 102.2 |
| Al-7075-T6 | 503 | 2.81 | 179.0 |
| Ti-6Al-4V | 880 | 4.43 | 198.7 |
| CFRP | 600 | 1.55 | 387.1 |

### 3.2.2 Determining Dimensional Stability (Resistance to Thermal Expansion)

Considering the large temperature range the small satellite will encounter while on its journey through the GEO (from $-150^{\circ}C$ to $150^{\circ}C$), it must be durable against temperature related deformations. Dimensional stability is defined as a material's ability to withstand thermal deformation when subjected to extreme temperatures. This property in materials can be modeled through the coefficient of thermal expansion (CTE):

$$\alpha = \frac{\Delta L}{L \Delta T}$$

The docking process necessitates precise alignment, thus keeping it structurally similar is incredibly important. Materials with smaller CTE values expand less under temperature change, helping maintain alignment and structure in the smallsat throughout its mission.

### 3.2.3 Determining Thermal Spreading Capability

Thermal spreading determines how well a material conducts and distributes heat. In a metal, thermal spreading can be determined through finding its thermal conductivity (k):

$$k = \frac{-q}{\nabla T}$$

Materials with a higher thermal conductivity can distribute heat more effectively. This leads to less heat accumulation in certain pockets of the spacecraft, known as "thermal hotspots", which could damage both the structure of the spacecraft at those points and electronics housed inside [19].

**Table 5. Thermal Conductivity of Materials [19][20][21]**

| Material | Thermal Conductivity |
|---|---|
| Aluminum 6061-T6 | 167 |
| Aluminum 7075-T6 | 130 |
| Ti-6Al-4V | 6.7 |
| CFRP | 5 |

### 3.2.4 Determining Radiation Shielding Efficiency

The radiation shielding capabilities of a material are directly proportional to its density. The higher the density of the material, the greater attenuation per unit thickness.

**Table 6. Density of Materials [16][18]**

| Material | Density (g/cm^3) |
|---|---|
| CFRP | 1.55 |
| Al-6061-T6 | 2.70 |
| Al-7075-T6 | 2.81 |
| Ti-6Al-4V | 4.43 |

While material shielding is effective, radiation protection is primarily achieved through external shielding. MLI blankets, which are multiple (usually 5-30 layers) thin, reflective sheets of aluminized Mylar, draped onto the outer shell of the smallsat reduce radiative heat transfer by essentially reflecting radiation away from the satellite [22].

**Table 7. Chassis Material Trade Study**

| Criterion | Weight | Al 6061-T6 | Al 7075-T6 | Ti-6Al-4V | CFRP |
|---|---|---|---|---|---|
| **C1 Strength / Weight** | 31.25% | 2.6 | 4.6 | 5.1 | 10.0 |
| **C2 Dimensional Stability** | 31.25% | 0.4 | 0.4 | 1.2 | 10.0 |
| **C3 Thermal Spreading** | 18.75% | 10.0 | 7.8 | 0.4 | 0.3 |
| **C4 Radiation Shielding** | 18.75% | 6.1 | 6.3 | 10.0 | 3.5 |

Results: CFRP - 8.30/10, Ti-6Al-4V - 5.52/10, Al 7075-T6 - 5.15/10, Al 6061-T6 - 4.77/10

### 3.2.5 Hybrid Material Approach

While CFRP has the highest score, some of the other materials have much higher scores in other categories. Thus, a targeted multi-material approach to building the chassis would be the most optimal for a balance of durable performance, thermal and radiation management.

Thus, the final structural design would incorporate:

- CFRP Primary Structural Members
- Aluminum equipment panels
- Titanium interfaces in high stress regions such as the chassis connection to the docking ring, tank mounting brackets and forward bulkhead behind the docking ring
- MLI Blanket

## 3.3 Bill of Material and Estimated Mass

A preliminary bill of materials (BOM) was developed to estimate both the mass and cost of the chassis structure for the smallsat. This BOM is calculated based on interface assumptions from other subteams, along with the reference used for the estimate. Simple parts like pressure vessels and covers are priced from industry suppliers. All prices had a factor added, and were additionally rounded up.

**Table 8. Bill of Materials [26][27][28][29][30][31]**

| # | Component | Basis / COTS reference | Mass (kg) | Est. cost ($) | Notes |
|---|---|---|---|---|---|
| **Refueling system** | | | | | |
| 1 | Xenon accumulator (COPV, 0.3 m³) | ESA L-XTA heritage | 22.0 | $180,000 | Ti liner + CFRP overwrap |
| 2 | Xenon propellant (210 kg) | Propulsion-grade Xe | 210.0 | $630,000 | ~$3,000/kg market rate |
| 3 | High-pressure He cylinder | COTS COPV | 8.0 | $45,000 | Client tank pressurization |
| 4 | Valves, regulators, feed lines | Moog / Vacco heritage | 6.5 | $120,000 | Solenoid, check, relief valves |
| 5 | Pressure & temp instrumentation | COTS transducers | 1.5 | $25,000 | PTs, thermocouples, flow sensor |
| 6 | Docking interface (client-side) | SM design, machined | 3.0 | $15,000 | Pre-launch install on client |
| **Docking system** | | | | | |
| 7 | SM hexagonal mechanism | Custom (Orbit Fab ref.) | 12.0 | $250,000 | 3 claws + spring locks |
| 8 | Docking sensors (LIDAR + camera) | COTS prox. sensors | 4.0 | $180,000 | RPO sensor suite |
| **GNC & propulsion** | | | | | |
| 9 | Hall-effect thruster | Busek BHT-600 | 8.0 | $350,000 | Includes PPU & cathode |
| 10 | Own-use Xe tank (50 kg cap.) | COTS COPV | 6.0 | $55,000 | MEO-to-GEO transfer fuel |
| 11 | Star trackers (x2, redundant) | Blue Canyon NST | 1.0 | $120,000 | Attitude determination |
| 12 | IMU + reaction wheels (x4) | Honeywell / NewSpace | 8.0 | $200,000 | 3-axis + 1 redundant |
| 13 | Flight computer (primary + backup) | RAD750 / LEON-class | 3.0 | $250,000 | Radiation-hardened |
| **Electrical power system** | | | | | |
| 14 | Triple-junction GaAs solar arrays | Spectrolab UTJ | 18.0 | $400,000 | ~2 kW BOL, deployable |
| 15 | Li-ion battery pack | EaglePicher / SAFT | 15.0 | $150,000 | Eclipse ops, ~2 kWh |
| 16 | PMAD (regulated bus, PCU, DC-DC) | GEOStar-2 heritage | 10.0 | $200,000 | 28V regulated bus |
| **Electrical power system** | | | | | |
| 14 | Triple-junction GaAs solar arrays | Spectrolab UTJ | 18.0 | $400,000 | ~2 kW BOL, deployable |
| 15 | Li-ion battery pack | EaglePicher / SAFT | 15.0 | $150,000 | Eclipse ops, ~2 kWh |
| 16 | PMAD (regulated bus, PCU, DC-DC) | GEOStar-2 heritage | 10.0 | $200,000 | 28V regulated bus |
| **Communications** | | | | | |
| 17 | S-band transponder + LGA | L3Harris / Gen. Dynamics | 5.0 | $180,000 | TT&C uplink/downlink |
| 18 | X-band transmitter + HGA | COTS X-band payload | 8.0 | $250,000 | High-rate data downlink |
| 19 | RF filters, diplexers, cabling | COTS | 3.0 | $40,000 | Signal chain components |
| **Chassis structure** | | | | | |
| 20 | CFRP central spine + internal frames | MEV/GEOStar-3 ref. | 26.7 | $5,848 | $219/kg catalog pricing |
| 21 | Ti-6Al-4V interfaces (bulkhead, brackets | MEV ref. | 11.6 | $1,673 | $144/kg catalog pricing |
| 22 | Al-6061-T6 panels & enclosures | MEV ref. | 26.8 | $887 | $33/kg catalog pricing |
| 23 | MLI blankets + fasteners/misc. | COTS | 2.0 | $1,500 | Thermal + radiation |
| **Integration, assembly & test (IA&T)** | | | | | |
| 24 | System integration & testing | Industry estimate | | $300,000 | ~8% of hardware cost |
| | **TOTAL (dry mass, excl. Xe propellant)** | | **393** | **$3,949,908** | |

Total Cost = $3,949,908

This BOM cost estimate is a preliminary estimate based on publically available catalog info, and is not a fabricated flight hardware quote.

## 4. Electrical Systems

The electrical system is responsible for continuous power generation, storage, management, and distribution for all spacecraft subsystems throughout the 10-15 year design life in GEO. The system must maintain stable bus voltage for noise-sensitive RF electronics, withstand cumulative radiation exposure, support both sunlit and eclipse operations (up to ~70 minutes per day near equinoxes), and provide fault protection, including overcurrent protection and redundancy for critical systems [32].

To determine the optimal electrical system architecture, trade studies were conducted on PMAD architectures and power generation methods, as outlined in the following sections.

### 4.1.1 Trade Study of PMAD Architecture

Every satellite or spacecraft must have a power management and distribution (PMAD) system architecture [32].

The two main options for an effective PMAD system are either regulated power busses or unregulated power busses. A regulated power system will use a main PCU (power conditioning unit) and DC-DC converters to produce usable fault-tolerant voltages for the system [33]. However, this will make the power system less efficient, as it needs to go through more components and processes before reaching each of the subsystems. Not only that, but it will also make the system weigh more, due to more steps in the process [37]. One example of this being used is the GEOStar-2 created by Northrop Grumman Innovation Systems.

The other option is the unregulated power bus architecture. This system is designed so that each bus is tied directly to the battery/solar array process, with no regulation or filtering of power [33]. The regulation of the current is handled at the load level and used for a satellite with less sensitive sensors/technology; however, this allows for more possible faults and unstable voltage. The system is more efficient, though, and maximizes both cost effectiveness and the system's size/weight due to fewer components and processes being required [37].

The selection criteria used were ranked out of 10 based on fault tolerance, efficiency, cost, size/weight, and voltage stability. While the regulated power system did outperform the unregulated in fault tolerance and voltage stability metrics, it underperformed comparatively in efficiency, cost, and size/weight selections. The final percentage was 75.5% for regulated, and 76% for unregulated. This demonstrates that either of these solutions will work for the satellite; it depends on the main mission, weighing between cost and risk [32].

### 4.1.2 Trade Study of Power Generation Methods

To operate efficiently, a satellite must have a method of power generation to be able to allocate enough voltage to each subsystem [36]. Additionally, the power generation method must minimize mass and volume for launch/stability. Temperature is another important factor in space, because when the satellite orbits around our Earth, it goes through 16 sun cycles in a day, and it will see temperatures as low as -170 C and as high as 120 C [36]. As it orbits, it goes through periods of direct sunlight with no atmosphere, and periods of cold space with no sunlight visible. However, if the power generation method is compatible with the power architecture and battery charging, a solar cell will operate efficiently when in view of the sun, and will store up energy for its dark periods [37].

Two popular options for various spacecraft's solar arrays are Triple-Junction GaAs solar cells and Crystalline Silicon solar cells. Although they have many differences, they both are efficient methods of gathering energy for a satellite, and can be used in many different applications [34].

The Triple-Junction GaAs solar cell works by having multi-layered photovoltaic devices or cells that typically use GaAs, or Gallium Arsenide [35]. This compound is a semiconductor that is vital for high-speed electronics and is specialized for applications similar to satellites, due to its radiation-tolerant capabilities in radiation and harsh space environments [35]. These cells optimize sunlight conversions with their layered structure and will use a technique called spectrum splitting, where each layer is tuned to absorb a specific wavelength range of the sun to allow for maximum efficiency [35].

The other popular solar array option is the Crystalline silicon solar cell. They are by far the most common solar cells used on Earth, and are developed from highly pure silicon crystals that efficiently convert sunlight into electricity [36]. These solar cells have one layer of p-n junctions, which will absorb photons when sunlight strikes the cell, and then collect the electrons using the electric field in the p-n junction [36]. These free electrons

will create DC energy to be used for various subsystems. Although crystalline silicon solar cells are more cost-effective and dominant in the solar industry as a whole, they tend to have worse performance in extreme heat/low light conditions, and tend to have a shorter lifespan while in contact with constant radiation [34].

In the trade study, the criteria that were weighed were for voltage generation, cost, power-to-mass ratio, radiation tolerance, and thermal performance. After analysing each system and ranking each category out of 10, the Triple-Junction GaAs solar cells scored a 74%, while the Crystalline Silicon solar cells scored a 51.5%. Although the Crystalline Silicon solar cells are much cheaper and easier to produce, the Triple-Junction GaAs solar cells outperform the other in almost every category, making it a worthwhile investment if the funds or materials are available [35].

## Figure 6. Radiation Exposure Degradation to Solar Arrays

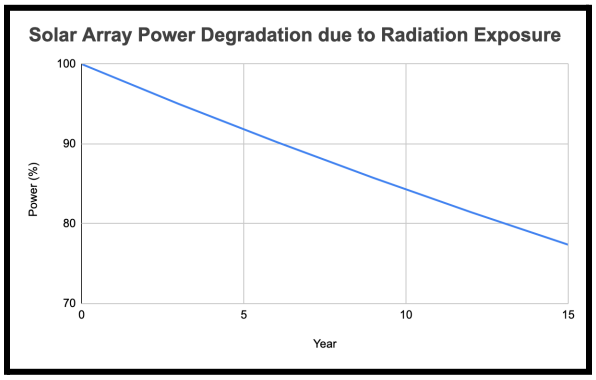


*Solar array power degradation due to radiation exposure over GEO mission lifetime, assuming ~5% degradation per year for triple-junction GaAs solar arrays. [38]*

## 4.2 Power Methodology

The electrical system will be organized into 4 main subsystems [32]. Each subsystem will operate together to provide continuous power in GEO.

The first subsystem is the power generation system, allowing deployable solar arrays to maintain adequate power resources on board [36]. This will be designed to meet BOL and EOL power requirements. These solar arrays will be high-efficiency triple-junction GaAs cells (1.1b) sized to provide operational load power and battery charging margin [35]. These solar arrays will be selected to maximize surface area and minimize launch volume. All output power from the solar arrays will be routed to the PMAD subsystem [37].

The second subsystem is the energy storage subsystem, where batteries sized for eclipse periods will allow the satellite to continue operations during these dark periods, with no external power entering the system [37]. This system will store excess energy generated by sunlight to support bus stability during transitions and be designed for a long life cycle, radiation tolerance, and thermal stability [32]. The battery output will be connected to the PMAD subsystem.

The third subsystem is the PMAD, which is the central part of the electrical power system [33]. This system will receive power from solar arrays/batteries and will perform voltage regulation, current limiting, and power routing with a regulated PMAD system [33]. Power will be routed and distributed to each subsystem: Refueling, docking, and other subsystems. The system will ensure stable bus voltage, noise filtering, and fault isolation [32].

The remaining subsystem is for the communication power interface. This subsystem is a dedicated interface for the RF payload [32]. It will provide stable, low-noise power and will support transponders, amplifiers, and all RF electronics. This subsystem is especially important as communication payload electronics are power-sensitive and noise-sensitive [32]. This might include additional filtering or a dedicated regulation stage to ensure continuous communication operation.

In this satellite system, there will be two power modes, sunlight mode and eclipse mode. During sunlight mode, the dollar arrays generate primary power, and the PMAD distributes power to loads, and the excess energy will charge the

batteries [37]. In the eclipse mode, the solar arrays will be inactive, and the batteries will provide power to PMAD to distribute power to subsystems to maintain continuous operations during the eclipse [37].

**Figure 7. Satellite Power Flow Chart**

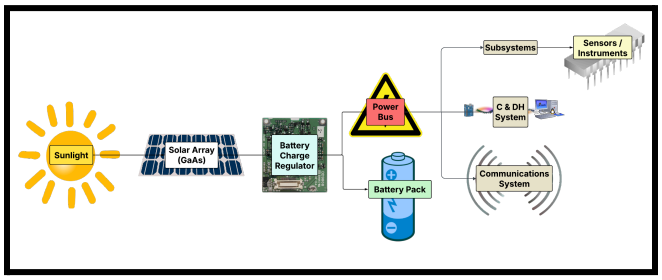


*Satellite power flow from solar arrays through regulation to spacecraft subsystems.*

### 4.3.1 Trade Study of Telecommunications Antenna

Every satellite requires reliable GEO communications to be able to operate via telemetry, commanding, and payload data support. The antenna must be able to provide a stable connection to the ground station while also minimizing mass/volume (for launch) and data losses [34]. Additionally, the antenna electronics must be able to tolerate radiation and single-event effects, while being aimed towards the ground station at all times.

Two antenna types were considered to allow this: High Gain Antenna (HGA) and Low Gain Antenna (LGA). The HGA provides high directional gain and is able to support higher data rate payload transmissions [34]. However, a main disadvantage to this is that the HGA requires very precise positioning towards Earth and much increased system complexity due to higher system-level amplifiers needed. The LGA provides wide RF coverage across Earth and allows reliable low data rate communications with minimal necessity of positioning requirements [34]. However, an LGA cannot support high data rate payload transmissions.

In this trade study, the criteria selected to determine and calculate the advantages and disadvantages of each antenna were based on Data Rate, Power Consumption, Cost, Size/Weight, Pointing Accuracy, and Reliability. After analysing each factor, while the HGA was at 54.5%, the LGA was determined to be the winner at 67% due to its reliability/signal integrity, along with its more efficient power consumption. While LGAs are better suited for CubeSats, most other satellites have both HGAs and LGAs for different purposes and for redundancy of telecommunications [34].

### 4.3.2 Trade Study of Telecommunications Operating Frequency

Operating frequency affects data rate transmissions, antenna size, and bandwidth [34]. Every satellite with telecommunications must provide stable and efficient communication to the ground station, while supporting commanding, telemetry, and data collection from the ground. The operating frequency must also minimize data losses while also tolerating radiation and atmospheric effects from downlinking.

For the satellite, two different frequencies were considered: S-band and X-band. S-band is within 2-4 GHz and will require less power and have lower atmospheric effects on data transmissions [34]. However, it has a low-moderate data rate with a larger antenna size and simpler data communications. For X-band, its frequency range is 8-12 GHz, with a higher data rate transmission and a smaller antenna size required [34]. However, X-band does come with more power and more complex electronics being required, and higher atmospheric effects.

The trade criteria selected for this trade study are Data Rate, Power Efficiency, Antenna Size, Atmospheric Loss, and Complexity. Looking at the differences between S-band and X-band, X-band was at 57%, while the S-band was determined to be the winner at 71.5% due to its more power/cost efficient properties, while also maintaining data/signal integrity [34].

## 4.4 Communications/RF Methodology

The communications subsystem allows telemetry, command, and payload data transmissions [34]. For the satellite mission, a dual-frequency architecture was selected using both S-band and X-band for different purposes. S-band operating frequency is being used for telemetry, tracking, and commanding through LGA, while the X-band operating frequency is being used for high data rate payload/refueling data transmission through the HGA [34]. The S-band will provide reliable low data rate communications and redundancy, while the X-band enables higher bandwidth directional downlink during operations.

The system uses a combination of HGA and LGA antennas for redundancy [34]. The HGA provides high data rate Earth-positioning communications, while the LGA provides wide coverage for safe mode and low data rate telemetry. The RF chain includes antennas, filters, amplifiers, and transponders [34]. Signals received from the ground station are processed on board and retransmitted via downlink. The stable power coming from the PMAD ensures low-noise RF performance [32]. The redundancy between HGA/LGA improves communication reliability over the mission lifetime [34].

**Figure 8. Dual-band Comm System Flow**

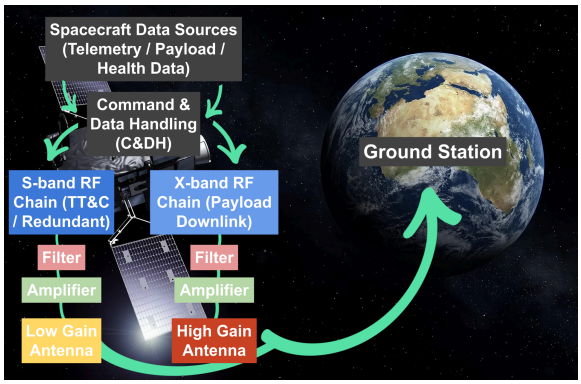


*Dual-band communication architecture using S-band LGA for telemetry, tracking, and commanding, and X-band HGA for high data rate payload downlink.*

## 5. GNC – MEO to GEO Rendezvous

To effectively rendezvous with the client satellite in GEO, a MATLAB simulation was developed to determine the optimal injection point from our spacecraft's initial orbit. This initial insertion orbit would realistically be MEO, as it is a common insertion point at high altitude for payloads such as our spacecraft. LEO insertion would be undesirable for the mission due to the large delta-V that would be required. This delta-V is determined by the Hohmann transfer, which was utilized as a function to find the necessary transfer time that would allow our spacecraft to inject into an orbital trajectory toward GEO, on path with our client satellite. Once the client satellite's position was initialized and chosen arbitrarily in GEO, a universal variables function was used to find its terminal position over the time span of the Hohmann transfer period. Then, a loop was created to iteratively solve for the proper injection point in MEO to meet the satellite at the terminal rendezvous point. The MEO insertion point of the spacecraft could be pre-determined from a desired launch of payload delivery. A Lambert solver could then be used to determine the delta-V under a desired lead time necessary to reach the injection point for trajectory to the rendezvous point.

**Figure 9. MATLAB Simulation of Rendezvous**

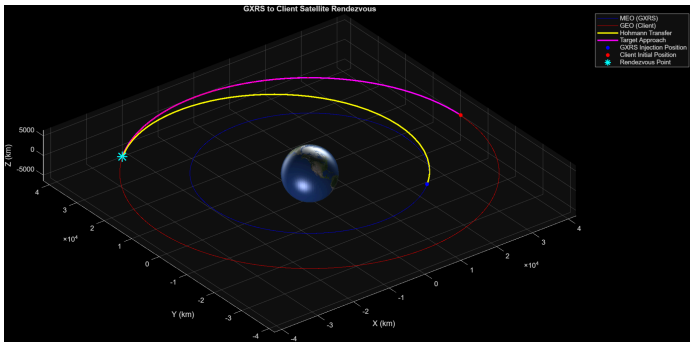


## Sources:

[1] C. W. Pierce, P. S. McRight, and J. Stephens, *A Review of In-Space Propellant Transfer Capabilities and Technologies*, NASA Technical Publication, 2020, sec. 2.2.3.3. [Online]. Available:

https://ntrs.nasa.gov/api/citations/20205007997/downloads/11-7-24%2020205007997.pdf. Accessed: Jan. 2026.

[2] NASA, *State-of–the-Art in Small Spacecraft Propulsion*, 4.6.2 In-Space Electric Propulsion, NASA Small Spacecraft Technology Program, Feb. 14, 2025. [Online]. Available: https://www.nasa.gov/smallsat-institute/sst-soa/in-space_propulsion/#4.6.2. Accessed Jan. 2026.

[3] N. Fazio, S. B. Gabriel, I. O. Golosnoy, and B. Wollenhaupt, "Mission cost for gridded ion engines using alternative propellants," in *36th International Electric Propulsion Conference (IEPC)*, Vienna, Austria, Sep. 15–20, 2019. [Online]. Available: https://electricrocket.org/2019/831.pdf. Accessed Jan. 2026.

[4] European Space Agency, *Use of Iodine as Propellant for Hall Effect Thrusters*, Programme T719-501MP, SITAEL S.p.A., 2017–2021. [Online]. Available: https://nebula.esa.int/content/use-iodine-propellant-hall-effect-thrusters. Accessed: Jan. 2026.

[5] J. Szabo, R. Tedrake, G. Kolencik, and B. Pote, *Measurements of a Krypton Fed 1.5 kW Hall Effect Thruster with a Centrally Located Cathode*, in *35th International Electric Propulsion Conference (IEPC 2017)*, Georgia Institute of Technology, Atlanta, GA, USA, Oct. 8–12, 2017. [Online]. Available: https://electricrocket.org/IEPC/IEPC_2017_26.pdf. Accessed: Jan. 2026.

[6] A. Morales, "Satellite Temperature Modeling in Geostationary Orbit Using COMSOL," ResearchGate, Dec. 2023. [Online]. Available: https://www.researchgate.net/publication/376187155_Satellite_Temperature_Modeling_in_Geostationary_Orbit_Using_COMSOL. Accessed: Jan. 2026.

[7] Quality Hydraulics & Pneumatics, "Sizing Hydraulic Accumulators for Various Applications," *Quality Hydraulics & Pneumatics Blog*, [Online]. Available: https://www.qualityhydraulics.com/blog/accumulators/hydraulic-accumulator-sizing. Accessed: Jan. 2026.

[8] Orbit Fab, "RAFTI User Guide," 2022. [Online]. Available: https://www.orbitfab.com/wp-content/uploads/DOC-00012-A_RAFTI_User_Guide.pdf

[9] Autonomous Satellite Servicing and Propellant Transfer (ASPN) Standard, "ASPN-STD-001 Rev-," [Online]. Available: https://517792.fs1.hubspotusercontent-na1.net/hubfs/517792/Space/MAP%20Standard/ASPN-STD-001_REV-.pdf

[10] F. Xijun, Z. Yuege, and N. Tigang, "Analysis of optical fiber performance at extreme temperature in low earth orbit," *Optik*, vol. 250, p. 168344, Jan. 2022, doi: https://doi.org/10.1016/j.ijleo.2021.168344.

[11] NASA Earth Observatory, "Probing the Electric Space Around Earth," *NASA Science*, Aug. 31, 2012. https://science.nasa.gov/earth/earth-observatory/probing-the-electric-space-around-earth-78985.

[12] "MEV-1 & 2 (Mission Extension Vehicle-1 and -2)," *www.eoportal.org*, Mar. 25, 2025. https://www.eoportal.org/satellite-missions/mev-1

[13] Northrop Grumman, "Pioneering the Future of Space MISSION EXTENSION VEHICLE (MEV) Award-Winning Satellite-Life-Extension Servicing Vehicle," 2021. Available: https://cdn.northropgrumman.com/-/media/wp-content/uploads/Mission-Extension-Vehicle-MEV-fact-sheet.pdf?v=1.0.0

[14] P. Amadieu, G. Beckwith, J. P. Bouchery, and V. Pery, "Figure 1. ATV approaches the ISS," 2002. Accessed: Apr. 08, 2026. [Online]. Available: https://www.esa.int/esapub/bulletin/bullet111/chapter17_bul111.pdf?

[15] NASA, "Optics - NASA Science," *science.nasa.gov*, Jan. 18, 2024.

https://science.nasa.gov/mission/hubble/observatory/design/optics/

[16] "Specific Material Search," *Matweb*. https://asm.matweb.com/search/specificmaterial

[17] Thyssenkrupp, "7075 Aluminium vs 6061 Aluminium," *Materials UK*. https://www.thyssenkrupp-materials.co.uk/technical-knowledge-hub/7075-aluminium-vs-6061-aluminium

[18] B. Bhat and A. Pandey, "Aerospace Materials Characteristics," *NASA*, 2025. https://ntrs.nasa.gov/api/citations/20180001137/downloads/20180001137.pdf

[19] "Understanding the Carbon Fibre Thermal Expansion Coefficient: A Comprehensive Guide - China carbon fiber drone products, carbon fiber, aramid fiber products and customized manufacturers," *China carbon fiber drone products, carbon fiber, aramid fiber products and customized manufacturers*, Aug. 04, 2025. https://sinocarbonfibre.com/understanding-the-carbon-fibre-thermal-expansion-coefficient-a-comprehensive-guide/

[20] "6061 Aluminum: Get to Know its Properties and Uses ," *Gabrian*, Feb. 12, 2019. https://www.gabrian.com/6061-aluminum-properties/

[21] Engineering ToolBox, "Thermal Expansion of Metals," *Engineeringtoolbox.com*, 2011. https://www.engineeringtoolbox.com/thermal-expansion-metals-d_859.html

[22] "Multi layer Insulation & Multilayer Film Materials ," *Dunmore*, 2015. https://www.dunmore.com/products/multi-layer-films

[23] NASA, "State of the Art of Small Spacecraft Technology," *NASA*, Mar. 08, 2024. https://www.nasa.gov/smallsat-institute/sst-soa/structures-materials-and-mechanisms/

[24] T. Hanada and K. Maniwa, "How Small Satellites Can Comply with the Space Debris Mitigation Guidelines?," Jun. 2011. https://www.researchgate.net/publication/272791028_How_Small_Satellites_Can_Comply_with_the_Space_Debris_Mitigation_Guidelines

[25] M. Glogowski, J. Anderson, G. Herbert, A. Kodys, and W. Llorens, "Application of Solar Electric Propulsion in the Emerging Satellite Servicing Industry," 2019. Accessed: Apr. 08, 2026. [Online]. Available: https://electricrocket.org/2019/753.pdf

[26] "0.19" Aluminum Sheet 6061-T6 | Online Metals," *Online Metals*, 2026. https://www.onlinemetals.com/en/buy/aluminum/0-19-aluminum-sheet-6061-t6/pid/1247?srsltid=AfmBOop7vX6nJ5UxT-YAY6h_gBOY1keWHX4ngKFus7UnMVcCnXa4VZla (accessed Apr. 08, 2026).

[27] "3/8" Aluminum Plate 7075-T651 | Online Metals," *Online Metals*, 2026. https://www.onlinemetals.com/en/buy/aluminum/0-375-aluminum-plate-7075-t651/pid/10437?srsltid=AfmBOoqIGZVdMuaQOFSEiDMx_ualybAw_dxZM6w79sQ1BoCq4oiFzgLO (accessed Apr. 08, 2026).

[28] "1/8" 6Al-4V Titanium Sheet Grade 5 | AMS-2631," *Online Metals*, 2026. https://www.onlinemetals.com/en/buy/titanium/0-125-titanium-sheet-grade-5-6al-4v/pid/mp-00003661?srsltid=AfmBOop-dDqNFLv0WX6F4MqAqE_PRVtD4zZ_eNAqpy6v5S2coVwx-wH0 (accessed Apr. 08, 2026).

[29] "DragonPlate | Engineered Carbon Fiber | Made in USA," *Dragon Plate*, 2026. https://dragonplate.com/15mm-quasi-isotropic-carbon-fiber-sheets?srsltid=AfmBOordzYbYpwPaRdKUpotLDBAsgqQcx4aE-dth0pdYfmR8S7Q5wRnu (accessed Apr. 08, 2026).

[30] "Custom Thermal Insulation & MLI Blankets," *SatBase*, Jan. 19, 2026.

https://satbase.com/catalog/item/txi_v5XHBT3EUEQ4/custom-thermal-insulation-mli-blankets (accessed Apr. 08, 2026).

[31] Military Fasteners, "NAS8803A6 Bolt - titanium alloy," *Military Fasteners*, 2026. https://military-fasteners.com/bolts/close%2Btolerance%2Bbolts/nas8803a6 (accessed Apr. 08, 2026).

[32] K. Eckles, "Key Considerations for Advancing Satellite Electrical Power Systems." Accessed: Jan. 16, 2026. [Online]. Available: https://www.ti.com/lit/ta/sszt054/sszt054.pdf?ts=1766139092692

[33] D. Olsson, "The 100 Volt Power Bus - More Than a Higher-Voltage." https://articles.adsabs.harvard.edu/cgi-bin/nph-iarticle_query?1998ESASP.416..237O&defaultprint=YES&filetype=.pdf

[34] S. Caldwell, "State-of-the-Art of Small Spacecraft Technology," *NASA*, Oct. 27, 2021. https://www.nasa.gov/smallsat-institute/sst-soa/

[35] M. Wanlass et al., "ULTRA-THIN, TRIPLE-BANDGAP GaInP/GaAs/GaInAs MONOLITHIC TANDEM SOLAR CELLS." Accessed: Jan. 16, 2026. [Online]. Available: https://ntrs.nasa.gov/api/citations/20090022281/downloads/20090022281.pdf

[36] Amosborne, "Design Considerations for a Spacecraft Solar Array," *Osborne Electrical Engineering - Electrical Engineering Blog by Alex Osborne*, Dec. 04, 2023. https://www.osborneee.com/spacecraft-solar-array/

[37] J. Lee, E. Kim, and K. Shin, "Design and Management of Satellite Power Systems." Accessed: Jan. 16, 2026. [Online]. Available: https://rtcl.eecs.umich.edu/papers/publications/2013/main_satellite.pdf

[38] A. R. Lozinski, R. B. Horne, S. A. Glauert, Giulio Del Zanna, D. Heynderickx, and Hugh, "Solar Cell Degradation Due to Proton Belt Enhancements During Electric Orbit Raising to GEO," Space Weather, vol. 17, no. 7, pp. 1059–1072, Jun. 2019, doi: https://doi.org/10.1029/2019sw002213.